Title

Aptamer-based multifunctional ligand-modified UCNPs for targeted PDT and bioimaging

Journal

Nanoscale, 10(23)

ISSN

2040-3364

Authors

Hou, Weijia
Liu, Yuan
Jiang, Ying
et al.

Publication Date

2018-06-14

DOI

10.1039/c8nr01096j

Peer reviewed

HHS Public Access

Author manuscript

Nanoscale. Author manuscript; available in PMC 2019 June 14.

Published in final edited form as:

Nanoscale. 2018 June 14; 10(23): 10986–10990. doi:10.1039/c8nr01096j.

Aptamer-based, multifunctional ligand-modified UCNPs for targeted PDT and bioimaging

Weijia Hou[‡,a], **Yuan Liu**[‡,a,b], **Ying Jiang**[a,b], **Yuan Wu**[a,b], **Cheng Cui**[a], **Yanyue Wang**[a], **Liqin sZhang**[a], **I-Ting Teng**[a], and **Weihong Tan**[a,b]

[a]Department of Chemistry and Physiology and Functional Genomics, Center for Research at the Bio/Nano Interface, Health Cancer Center, University of Florida, Gainesville, FL 32611-7200, USA

[b]Molecular Science and Biomedicine Laboratory, State Key Laboratory of Chemo/Bio-Sensing and Chemometrics, College of Biology and College of Chemistry and Chemical Engineering, Hunan University, Changsha, 410082, China

Abstract

We designed an aptamer-based multifunctional ligand which, upon conjugation to the surface of upconversion nanoparticles (UCNPs), could realize phase transfer, covalent photosensitizer (PS) loading, and cancer cell targeting in one simple step. The as-built PDT nanodrug is selectively internalized into cancer cells and exhibits highly efficient and selective cytotoxicity.

Graphical Abstract

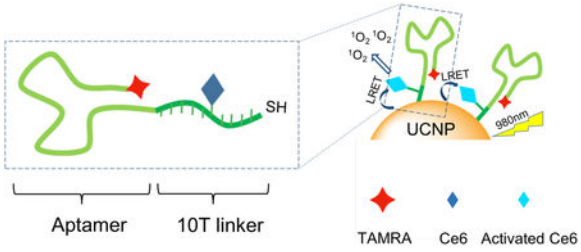

A multifunctional aptamer-based ligand is designed for surface modification of UCNPs to build an NIR-triggered PDT nanodrug.

Photodynamic therapy (PDT) includes three components: light, photosensitizer (PS) and oxygen.[1] Upon activation by photon absorption, the photosensitizer interacts with molecular oxygen to generate cytotoxic reactive oxygen species (ROS), which damage biomolecules in cells and causing cell death.[2, 3] Because of its advantages of high spatiotemporal specificity, high efficiency, and noninvasiveness, PDT has recently been extensively studied for cancer treatment. However, most photosensitizers currently used are excited by UV/Vis light, which

‡ These authors contributed equally to this work.

Electronic Supplementary Information (ESI) available: [details of any supplementary information available should be included here]. See DOI:10.1039/x0xx00000x

Conflicts of interest

There are no conflicts to declare.

has very short penetration depth in tissue, and the high energy may even damage healthy cells. To expand the application of PDT to deeper tumors and increase its biocompatibility, upconversion nanoparticles (UCNPs) have been utilized as an energy transducer to upconvert NIR light in the “biological window” (700–1300 nm) to shorter wavelengths.[4–7] This energy can be absorbed by the PS in the presence of a large overlap of the UCNP emission peak and PS absorption peak. Many publications have focused on hybridizing PS with UCNP to build an NIR light-triggered PDT nanodrug system. Since most UCNPs are synthesized and dispersed in organic solvents, the particles must be transferred to an aqueous phase for biocompatibility. The PS should also be stably loaded on the surfaces of UCNPs to achieve efficient luminescence resonance energy transfer (LRET). Several methods of loading UCNPs with PS, as well as making them water-soluble, have already been studied: polymer coating,[8–10] silica coating,[11–14] chemical linkage,[15, 16] physical adsorption,[17, 18] and electrostatic interaction.[19] However, such coatings usually constrain ROS diffusion from the nanoparticle surface, which is essential for PDT, since cytotoxicity is attributed to ROS and its interaction with biological substrates. Porous coating and adsorption methods commonly lead to unstable loading, and PS leakage may reduce therapeutic efficiency and increase side effects.

To address these obstacles, the present study reports the development of an aptamer-based multifunctional ligand for hybridization to UCNP surfaces to realize phase transfer, PS loading, and selective targeting with one simple thiol-ene click reaction. Aptamers are short DNA oligomers, whose secondary structures recognize target ions, biomolecules, and even cells.[20–25] Sometimes called synthetic antibodies, aptamers are much easier to functionalize than antibodies at precise sites.[26, 27] Thus, the photosensitizer Ce6 can be modified on an aptamer by chemical conjugation with controlled amount and position to develop a PS-loaded ligand. Very recently, our group developed a method using thiol-ene click reaction to orthogonally conjugate a thiol-modified aptamer onto a nanoparticle with high efficiency.[28] Taking advantage of this robust method, in one single step we covalently conjugated Ce6-modified aptamers onto the UCNP surface to build a biocompatible, highly efficient, and controllable NIR-activated PDT nanodrug able to recognize tumor cells with high selectivity. As shown in the Scheme, Ce6 is positioned close to the UCNP surface, which guarantees high LRET efficiency. Meanwhile, since Ce6 is covalently bonded to the nanoparticle, only negligible leakage of the PS is expected during storage or delivery. In addition, with no coating on the particle surface, the diffusion of O_2 and ROS is not blocked, which enhances the therapeutic efficiency of this nanodrug system. This nanoplatform can also be used for bioimaging with TAMRA dye labeled at the end of the aptamer.

The multifunctional DNA ligand (chemically synthesized with automated DNA synthesizer) is composed of three parts: the aptamer sequence with dye molecule for biotracking, a 10 T-base spacer with Ce6 coupling, and a thiol group at the 3-prime end for thiol-ene click conjugation. In this study, sgc8 aptamer was chosen as the model to study the specific binding and internalization behavior of the UCNP-Ce6-aptamer PDT nanosystem. Aptamer sgc8 has high binding affinity toward protein tyrosine kinase 7 (PTK7), which is overexpressed on the surface membrane of CCRF-CEM cells (human T-cell acute lymphocytic leukemia), but not Ramos cells.[23, 29, 30] Ten T bases were coupled to the 5-prime end of the sgc8 sequence as a spacer between the aptamer and particle surface. An

amine-modified T base (NH_2-dT) was coupled in the middle of the spacer sequence for further PS conjugation. The PS position was designed to be several nucleotides from the aptamer sequence to avoid interference with aptamer binding, while still located close enough to the UCNP surface to ensure efficient LRET between UCNP and PS, but without influencing the thiol-ene click reaction. The 5-prime end of the aptamer was coupled to a disulfide bond, which is reduced to a thiol group for efficient coupling to the particle's surface by a thiol-ene click reaction.

After synthesis and purification by HPLC, Ce6 was conjugated by EDC/NHS coupling between the carboxyl group on Ce6 and the amine group on NH_2-dT. The Ce6-conjugated product was separated from residual uncoupled DNA by HPLC, taking advantage of the hydrophobicity of Ce6. As shown in Figure S1, the HPLC chromatogram for DNA absorption (260 nm channel; green) shows two major elution peaks. The latter elution peak corresponds to the Ce6-coupled DNA, which also absorbs at 404 nm, the λ_{max} of Ce6. This assignment was further confirmed by the UV/Vis spectrum of the product (Fig. S2), showing characteristic peaks for DNA (260 nm), TAMRA (563 nm), and Ce6 (410 nm and 642 nm). Covalent attachment of the PS guarantees negligible leakage of PS and minimizes batch-to-batch variation of PS concentration, which is an essential factor for repeatable and accurate dosing in real applications. In addition, off-target toxicity caused by leakage of free PS is eliminated.

UCNPs ($NaYF_4$: Yb^{3+}30%, Er^{3+}2%) were synthesized as previously reported.[31] Dopamine acrylamide was used to conduct ligand exchange with oleic acid on the UCNP surface in order to modify a double bond onto the nanoparticle's surface.[28] The disulfide group on the 5' -end of the Ce6-conjugated aptamer ligand was reduced to a thiol group, which then reacted with the double bond on UCNP for a thiol-ene click reaction. The DNA ligands on the surface transfer hydrophobic UCNP to the aqueous phase, while the negative charge of DNA molecules keeps the UCNPs from aggregating. The photosensitizers were linked very close to the UCNP surface to ensure significant LRET. Furthermore, the sgc8 segment endowed the UCNP with specific recognition ability towards the CEM target cells to improve therapeutic performance. TEM images show that the synthesized nanoparticles are uniform, with diameters approximately 55 nm, and the phase transfer process did not change the size or shape of the UCNPs (Fig. 1a and 1b).

Fluorescence spectra were measured after transfer of the particles to the aqueous phase. The emission band at λ=654 nm matches very well with the absorption band of Ce6 at λ=642 nm, as illustrated in Figure 1c, which shows overlapping peaks highlighted in light blue shadow. Peak overlap is crucial for this nanodrug system since it determines the energy transfer efficiency between UCNP and PS, which, in turn, influences therapeutic efficacy. This energy transfer process was further proven by the decrease in 654nm peak when Ce6 is coupled (Fig. S4a), as well as the emission color change of the UCNP. Upon excitation with 980 nm laser, the luminescence of the UCNP-Ce6-sgc8 is green (Fig. S4b), compared with UCNP-sgc8 without Ce6, which emits yellow fluorescence, owing to a combination of red and green (Fig. S4c). This indicates that the Ce6 efficiently absorbs the red fluorescence of the UCNP. In addition, hydrodynamic diameter and fluorescence intensity have no change over the physiological pH range, indicating the good stability of this nanodrug (Fig. S3).

Next, the production of cytotoxic singlet oxygen, which is directly related to therapeutic efficiency of this PDT nanosystem against cancer, was evaluated. Singlet oxygen sensor green (SOSG) can be selectively oxidized by singlet oxygen, and it emits green fluorescence similar to fluorescein.[32, 33] SOSG was utilized to assess the singlet oxygen generation of UCNP-Ce6-sgc8 upon excitation with a 980 nm laser for different accumulation times. As shown in Figure 1d, a 2-fold increase of fluorescence was observed over 40 min of excitation, indicating that the singlet oxygen had been successfully generated and that it diffused into solution to react with other molecules.

Having demonstrated that this nanodrug can photodynamically generate singlet oxygen for therapeutic aims, we next examined its specific recognition toward positive cancer cells, which is highly important for increasing therapeutic efficiency, as well as eliminating deleterious effects toward nontarget tissue. Since aptamer Sgc8 was modified on the nanoparticle surface, CEM cells were selected as the positive cell line, and nonbinding Ramos cells were used as negative control TAMRA was labeled on DNA to track the nanoparticle by fluorescence signal (all cells were purchased from ATCC, Manassas, VA). TMR-sgc8-UCNP (10 μg/mL) was incubated with CEM and Ramos cells and then analyzed by flow cytometry (Fig. 2a and 2b). CEM cells incubated with the nanoplatform show a large shift in TAMRA fluorescence compared to cells without treatment; however, for Ramos cells, not much difference is noted between the two groups. This result illustrates the strong selective binding of the aptamer on nanoparticles toward positive cells, rather than negative cells. After confirming selective recognition, we further studied the selective endocytosis of this nanodrug, which is a common route for sgc8-mediated internalization.[30, 34, 35] As shown in the confocal microscope images (Fig. 2c and 2d), CEM cells incubated with the nanosystem showed a strong TAMRA fluorescence, but for the negative Ramos cells, only minimal binding and internalization were observed. Considering these two results, it is clear that the targeting function of the aptamer is not influenced by the chemical modification nor by the thiol-ene click reaction. These results also indicate the potential use of this nanosystem as a targeted bioimaging probe.

After confirming the selective binding and internalization of this nanodrug, we finally investigated its NIR-triggered photodynamic therapeutic effect on cells. CEM and Ramos cells were treated with a series of concentrations of UCNPCe6-sgc8, followed by exposure to 0.6w/cm^2 980 nm laser light. A non-irradiated group of cells was carried throughout the procedure as a control experiment to evaluate the dark toxicity of this nanodrug. After further incubation for 48 hours, cell viability was evaluated by MTS assay (Fig. 3). Without excitation, cell viability was greater than 90% for both positive and negative cell lines, even at the high 100 μg/mL concentration of UCNP-Ce6-sgc8, indicating the low dark toxicity and good biocompatibility of this nanodrug. The safety of the 980 nm laser was proven by irradiating drug-free samples of the cells, and the cell viability for both cell lines was around 100%. However, with increasing doses of UCNP-Ce6-sgc8 and laser irradiation treatment, significantly reduced CEM cell viability was observed (Fig. 3a). When treated with 100 μg/mL nanodrug, the cell viability was reduced to as low as 10%, suggesting the high photodynamic therapeutic efficacy of the nanodrug. In contrast, the negative Ramos cell group showed negligible cytotoxicity (Fig. 3b). Taken together with the confocal result, we

can conclude that the aptamer ligand-modified nanodrug is not uptaken into Ramos cells, confirming the high selectivity of the nanodrug.

Conclusions

In summary, we have developed a multifunctional aptamer-based ligand for surface modification of UCNPs. It can realize phase transfer, conjugated PS loading and selective targeting in one simple step. The as-synthesized NIR-triggered PDT nanodrug showed high selectivity and high cell killing efficacy with relatively low particle concentrations. This good performance is attributed to (1) the controlled distance between UCNP and PS that enabled high energy transfer efficiency, (2) an unblocked nanoparticle surface that provides free diffusion of the ROS, (3) trivial PS leakage owing to covalent drug loading, and (4) highly selective internalization based on the recognition capability of the aptamers. For future study, optimization of PS loading, as well as in vivo therapeutic effect and biodistribution, will be further investigated. Owing to the high programmability of DNA, this method can also be applied to other NIR light-responsive delivery systems for various kinds of cargos, such as chemotherapeutic drugs, photothermal drug systems, and macromolecules.

Supplementary Material

Refer to Web version on PubMed Central for supplementary material.

Acknowledgements

The authors give special appreciation to Dr. K. R. Williams for useful suggestions in writing. This work is supported by grants awarded by the National Institutes of Health (GM079359, GM111386, and CA133086). It is also supported by the National Key Scientific Program of China (2011CB911000), NSFC grants (NSFC 21221003 and NSFC 21327009) and China National Instrumentation Program 2011 YQ03012412.

Notes and references

1. Nowis D, Makowski M, Stokłosa T, Legat M, Issat T and Gołąb J, Acta Biochimica Polonica, 2005, 52, 339–352. [PubMed: 15990919]
2. Celli JP, Spring BQ, Rizvi I, Evans CL, Samkoe KS, Verma S, Pogue BW and Hasan T, Chemical reviews, 2010, 110, 2795–2838. [PubMed: 20353192]
3. Konan YN, Gurny R and Allémann E, Journal of Photochemistry and Photobiology B: Biology, 2002, 66, 89–106.
4. Lucky SS, Soo KC and Zhang Y, Chemical reviews, 2015, 115, 1990–2042. [PubMed: 25602130]
5. Shen Y, Shuhendler AJ, Ye D, Xu J-J and Chen H-Y, Chemical Society Reviews, 2016, 45, 6725–6741. [PubMed: 27711672]
6. Chen G, Qiu H, Prasad PN and Chen X, Chemical reviews, 2014, 114, 5161–5214. [PubMed: 24605868]
7. Fan W, Bu W and Shi J, Advanced Materials, 2016, 28, 3987–4011. [PubMed: 27031300]
8. Wang C, Tao H, Cheng L and Liu Z, Biomaterials, 2011, 32, 6145–6154. [PubMed: 21616529]
9. Liu X, Que I, Kong X, Zhang Y, Tu L, Chang Y, Wang TT, Chan A, Löwik CW and Zhang H, Nanoscale, 2015, 7, 14914–14923. [PubMed: 26300064]
10. Wang X, Liu K, Yang G, Cheng L, He L, Liu Y, Li Y, Guo L and Liu Z, Nanoscale, 2014, 6, 9198–9205. [PubMed: 24980695]

11. Wang H, Han R.-l., Yang L.-m., Shi J.-h., Liu Z.-j., Hu Y, Wang Y, Liu S.-j. and Gan Y, ACS applied materials & interfaces, 2016, 8, 4416–4423. [PubMed: 26816249]
12. Zhang P, Steelant W, Kumar M and Scholfield M, Journal of the American Chemical Society, 2007, 129, 4526–4527. [PubMed: 17385866]
13. Kim J, Cho HR, Jeon H, Kim D, Song C, Lee N, Choi SH and Hyeon T, Journal of the American Chemical Society, 2017, 139, 10992–10995. [PubMed: 28737393]
14. Idris NM, Gnanasammandhan MK, Zhang J, Ho PC, Mahendran R and Zhang Y, Nature medicine, 2012, 18, 1580–1585.
15. Liu K, Liu X, Zeng Q, Zhang Y, Tu L, Liu T, Kong X, Wang Y, Cao F and Lambrechts SA, ACS nano, 2012, 6, 4054–4062. [PubMed: 22463487]
16. Sun M, Xu L, Ma W, Wu X, Kuang H, Wang L and Xu C, Advanced Materials, 2016, 28, 898–904. [PubMed: 26635317]
17. Li S, Cui S, Yin D, Zhu Q, Ma Y, Qian Z and Gu Y, Nanoscale, 2017, 9, 3912–3924. [PubMed: 28261736]
18. Cui S, Yin D, Chen Y, Di Y, Chen H, Ma Y, Achilefu S and Gu Y, ACS nano, 2012, 7, 676–688. [PubMed: 23252747]
19. Wang M, Chen Z, Zheng W, Zhu H, Lu S, Ma E, Tu D, Zhou S, Huang M and Chen X, Nanoscale, 2014, 6, 8274–8282. [PubMed: 24933297]
20. Ellington AD and Szostak JW, Nature, 1990, 346, 818–822. [PubMed: 1697402]
21. Tuerk C and Gold L, Science, 1990, 249, 505–510. [PubMed: 2200121]
22. Jiang Y, Shi M, Liu Y, Wan S, Cui C, Zhang L and Tan W, Angewandte Chemie International Edition, 2017, 56, 11916–11920. [PubMed: 28834063]
23. Shangguan D, Li Y, Tang Z, Cao ZC, Chen HW, Mallikaratchy P, Sefah K, Yang CJ and Tan W, Proceedings of the National Academy of Sciences, 2006, 103, 11838–11843.
24. Zhang L, Yang Z, Le Trinh T, Teng I, Wang S, Bradley KM, Hoshika S, Wu Q, Cansiz S and Rowold DJ, Angewandte Chemie International Edition, 2016, 55, 12372–12375. [PubMed: 27601357]
25. Li Z, Wang J, Li Y, Liu X and Yuan Q, Materials Chemistry Frontiers, 2018.
26. Cui C, Zhang H, Wang R, Cansiz S, Pan X, Wan S, Hou W, Li L, Chen M and Liu Y, Angewandte Chemie, 2017, 129, 12116–12119.
27. Wang Y, Wu C, Chen T, Sun H, Cansiz S, Zhang L, Cui C, Hou W, Wu Y and Wan S, Chemical science, 2016, 7, 6041–6049. [PubMed: 28066539]
28. Liu Y, Hou W, Sun H, Cui C, Zhang L, Jiang Y, Wu Y, Wang Y, Li J and Sumerlin BS, Chemical science, 2017, 8, 6182–6187. [PubMed: 28989650]
29. Shangguan D, Cao Z, Meng L, Mallikaratchy P, Sefah K, Wang H, Li Y and Tan W, Journal of proteome research, 2008, 7, 2133–2139. [PubMed: 18363322]
30. Xiao Z, Shangguan D, Cao Z, Fang X and Tan W, Chemistry-A European Journal, 2008, 14, 1769–1775.
31. Liu Y, Purich DL, Wu C, Wu Y, Chen T, Cui C, Zhang L, Cansiz S, Hou W and Wang Y, Journal of the American Chemical Society, 2015, 137, 14952–14958. [PubMed: 26562739]
32. Han D, Zhu G, Wu C, Zhu Z, Chen T, Zhang X and Tan W, ACS nano, 2013, 7, 2312–2319. [PubMed: 23397942]
33. Tang Z, Zhu Z, Mallikaratchy P, Yang R, Sefah K and Tan W, Chemistry–An Asian Journal, 2010, 5, 783–786.
34. Wu Y, Sefah K, Liu H, Wang R and Tan W, Proceedings of the National Academy of Sciences, 2010, 107, 5–10.
35. Zhu G, Zheng J, Song E, Donovan M, Zhang K, Liu C and Tan W, Proceedings of the national academy of sciences, 2013, 110, 7998–8003.

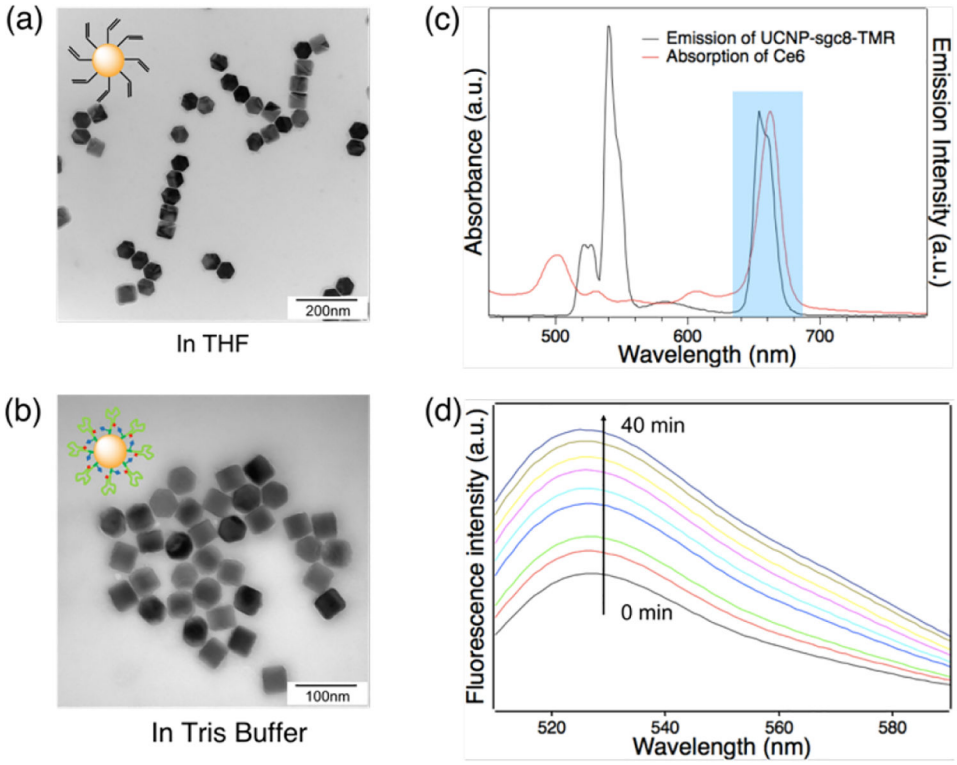

Fig 1.

Characterization of UCNP-sgc8-TMR. TEM images of UCNP (a) in THF before thiol-ene click reaction and (b) in Tris buffer after conjugation with DNA. (c) Emission spectrum of UCNP in water (black line) and UV/Vis absorption spectrum of Ce6 in ethanol (red line). The blue shadow indicates the overlapping peaks that contribute to LRET between UCNP and Ce6. (d) Monitoring singlet oxygen generation of UCNP-Ce6-sgc8 upon exciting with 980 nm laser (0.45 mW/cm^2) over a range of accumulation times: 0min, 5min, 10min, 15min, 20min, 25min, 30min, 35min, and 40min. The fluorescence arises from the reaction of singlet oxygen with SOSG.

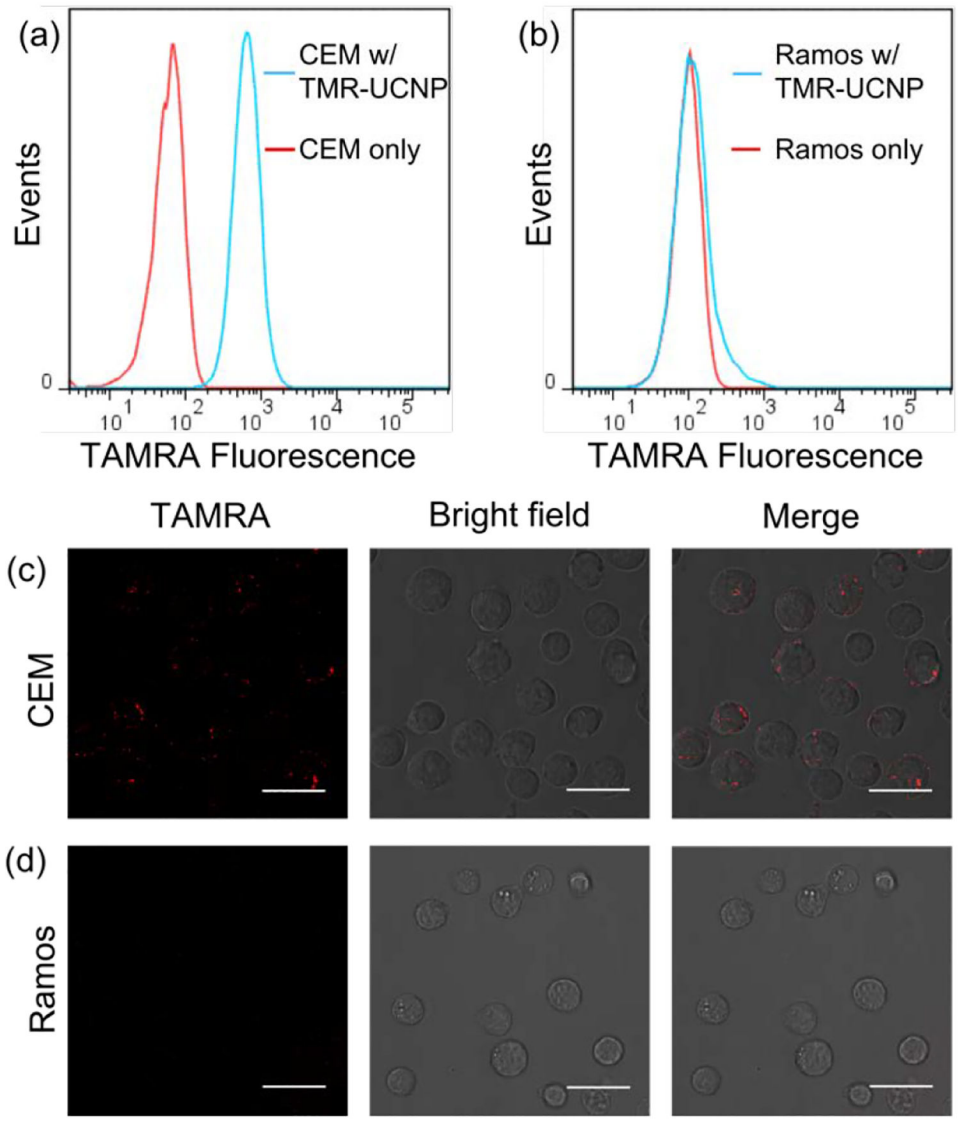

Fig 2.

Flow cytometry histogram of (a) CEM cells and (b) Ramos cells treated with the nanodrug. Confocal image of (c) CEM cell and (d) Ramos cell incubated with the nanodrug. Scale bar: 20 μm.

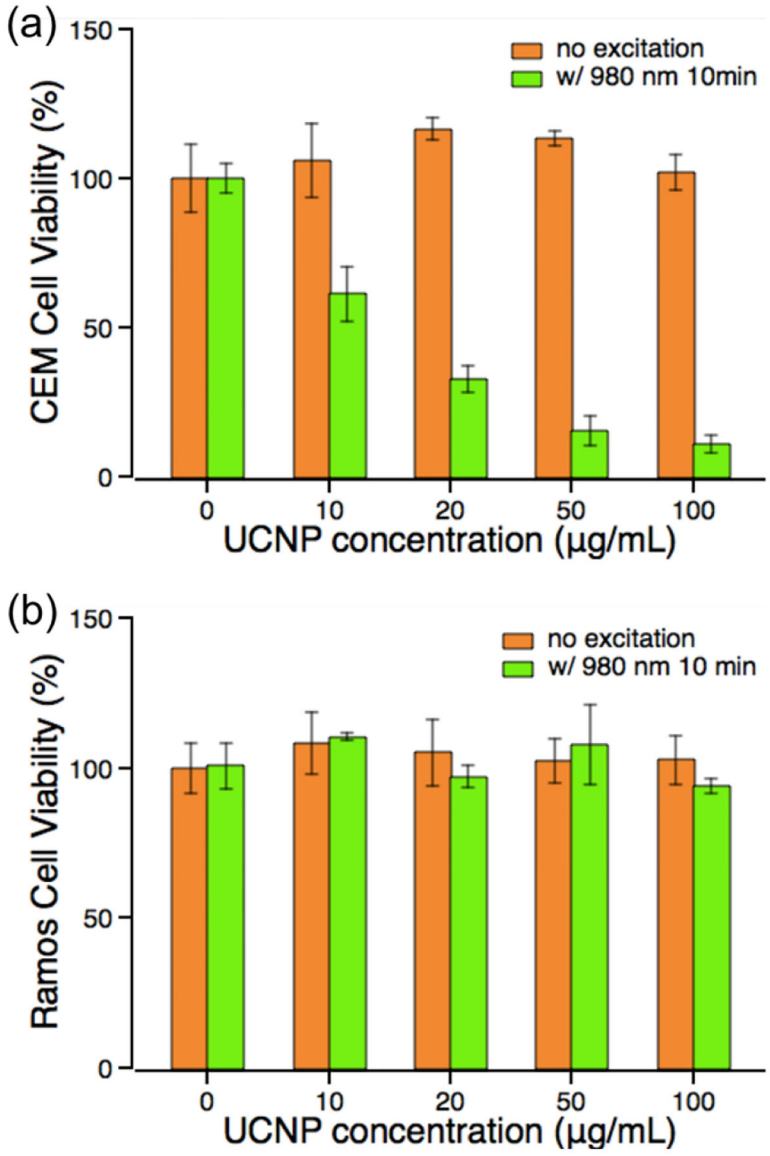

Fig 3.

Selective cytotoxicity of UCNP-Ce6-sgc8. MTS assay results of (a) CEM cells (target cells) and (b) Ramos cells (control cells) treated with UCNP-Ce6-sgc8 with 980nm laser (0.6 w/ cm2) excited for 10 min (green block) and without excitation (orange block).

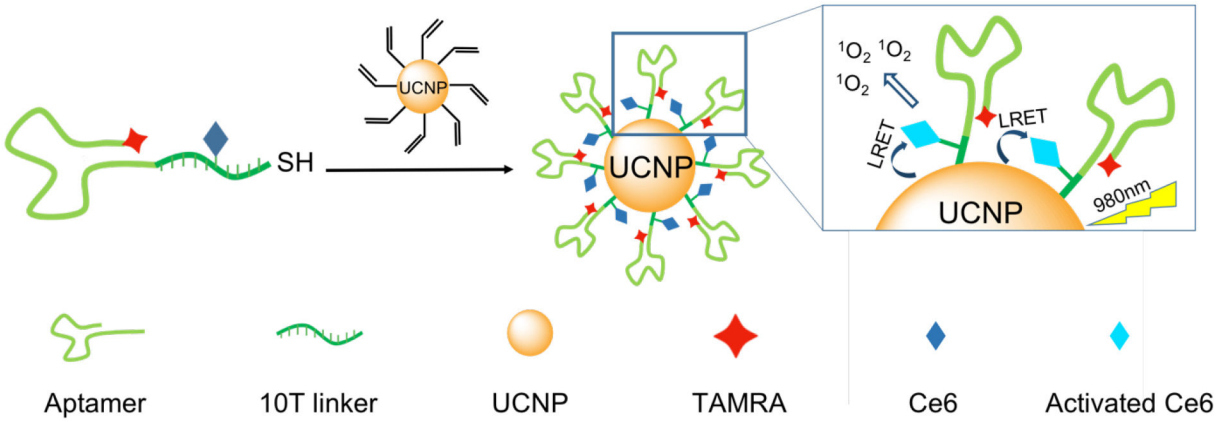

Scheme.

Schematic representation of UCNP-Ce6-aptamer synthesis and its singlet oxygen generation mechanism.